© 2021. Published by The Company of Biologists Ltd | Development (2021) 148, dev194571. doi:10.1242/dev.194571

STEM CELLS AND REGENERATION

RESEARCH ARTICLE

Proper timing of a quiescence period in precursor prospermatogonia is required for stem cell pool establishment in the male germline

Guihua Du[1,2], Melissa J. Oatley[2], Nathan C. Law[2], Colton Robbins[2], Xin Wu[1,*] and Jon M. Oatley[2,*]

ABSTRACT

The stem cell-containing undifferentiated spermatogonial population in mammals, which ensures continual sperm production, arises during development from prospermatogonial precursors. Although a period of quiescence is known to occur in prospermatogonia prior to postnatal spermatogonial transition, the importance of this has not been defined. Here, using mouse models with conditional knockout of the master cell cycle regulator *Rb1* to disrupt normal timing of the quiescence period, we found that failure to initiate mitotic arrest during fetal development leads to prospermatogonial apoptosis and germline ablation. Outcomes of single-cell RNA-sequencing analysis indicate that oxidative phosphorylation activity and inhibition of meiotic initiation are disrupted in prospermatogonia that fail to enter quiescence on a normal timeline. Taken together, these findings suggest that key layers of programming are laid down during the quiescent period in prospermatogonia to ensure proper fate specification and fitness in postnatal life.

KEY WORDS: Prospermatogonia, Quiescence, Spermatogonial stem cell

INTRODUCTION

Tissue-specific stem cells that support continual cycling of cell lineages through both self-renewal and production of differentiating progenitors are derived from precursors formed during embryonic, perinatal and neonatal development. These precursors progress through a diverse path of developmental milestones while gaining the capacity to support cell lineages long into adulthood. During development, precursors colonize different microenvironments, undergo epigenetic programming and dynamically alter proliferative states (Borgel et al., 2010; Saitou and Yamaji, 2012). A hallmark example of the latter is the perinatal mitotic arrest period of prospermatogonial precursors that occurs prior to formation of the undifferentiated spermatogonial population in which stem cell activity for the spermatogenic lineage is contained (Oatley and Brinster, 2008).

The subset of undifferentiated spermatogonia that possess stem cell activity is often referred to as spermatogonial stem cells (SSCs) and supports continuous spermatogenesis in adulthood (de Rooij and Russell, 2000; Oatley and Brinster, 2008). During development, SSCs originate from primordial germ cells (PGCs) that are induced from the proximal epiblast via WNT and bone morphogenetic protein signaling at embryonic day (E) 6.25 in mice (Lawson et al., 1999; Rivera-Perez and Magnuson, 2005). This signaling induction leads to the upregulation of *Blimp1* (also known as *Prdm1*), *Prdm14* and *Tfap2c*, which encode transcription factors that facilitate PGC specification, migration, and epigenetic reprogramming (Kurimoto et al., 2008; Magnusdottir et al., 2013; Yamaji et al., 2008). In subsequent developmental days, PGCs proliferate and migrate to the genital ridge (Hamer and de Rooij, 2018; Richardson and Lehmann, 2010). At E12.5 in mice, gonadal PGCs undergo sex determination in response to cues from the developing soma (Lin and Capel, 2015). If XX, germ cells initiate oogenesis and arrest in meiosis by E14.5 and remain in this state until puberty. By contrast, XY PGCs transition to form prospermatogonia, which continue to proliferate for several days before entering mitotic arrest around E16.5 (Saitou and Yamaji, 2012; Vergouwen et al., 1991). In the mouse, prospermatogonia progressively re-enter the cell cycle from postnatal day (P) 1.5-3.5 (Law et al., 2019). During this neonatal window, prospermatogonia transition to either from the foundational SSC pool that supports lifelong spermatogenesis or enter a differentiation pathway directly and contribute to a unique first round of spermatogenesis (Bellve et al., 1977; Law et al., 2019). Collectively, a variety of developmental milestones and dynamic cell-type transitions precede formation of the SSC population.

The fetal mitotic arrest and postnatal cell cycle re-entry periods of prospermatogonia are well-described developmental events, but the functional significance and key regulators of these processes have not been elucidated. During this period that precedes genesis of the spermatogenic lineage, prospermatogonia are known to re-establish DNA methylation patterns (Li and Sasaki, 2011), dynamically regulate histone modifications (Ly et al., 2015), migrate from the center of seminiferous cords to the basement membrane (Nagano et al., 2000), and preprogram postnatal SSC or differentiating fates (Law et al., 2019). At present, whether these processes and establishment of the spermatogenic lineage are tied to the mitotic arrest period or are developmentally independent is undefined.

Here, we used mouse models for conditional ablation of the master cell cycle regulator retinoblastoma transcriptional corepressor 1 (RB1) *in vivo* as a model system to explore the purpose of the prospermatogonial mitotic arrest period. Previous studies using *ex vivo* organ culture of testes from Rb1 null mouse fetuses indicate that PGC and prospermatogonial development are grossly normal but there is a delay in onset of the mitotic arrest (Spiller et al., 2010). As the previous studies did not create live animals with germ cell *Rb1* deficiency, ramifications of the delayed onset of mitotic arrest on establishment of the spermatogenic lineage and fertility in postnatal life remain undefined. The current study extends the foundational observations of Spiller et al. (2010) to show that conditional

[1]State Key Laboratory of Reproductive Medicine, Nanjing Medical University, Nanjing, Jiangsu, 211166, China. [2]School of Molecular Biosciences, Center for Reproductive Biology, College of Veterinary Medicine, Washington State University, Pullman, WA 99164, USA.

*Authors for correspondence (joatley@wsu.edu; xinwu@njmu.edu.cn)

M.J.O., 0000-0001-6692-4351; X.W., 0000-0001-7938-9407

Handling Editor: Haruhiko Koseki
Received 29 June 2020; Accepted 30 March 2021

Development (2021) 148, dev194571. doi:10.1242/dev.194571

inactivation of *Rb1* in germ cells starting at the PGC stage leads to impaired perinatal mitotic arrest of prospermatogonia and subsequent ablation of the germline *in vivo*, thereby causing sterility in postnatal life. In addition, outcomes of single-cell RNA-sequencing (scRNA-seq) analysis revealed that a metabolic shift occurs in prospermatogonia during the perinatal quiescence period that is disrupted in cells that fail to make this transition. Also, inhibition of meiotic entry is impaired in prospermatogonia that do not initiate mitotic arrest. Collectively, these findings suggest that the purpose of the mitotic arrest period in prospermatogonia is to set programming for the undifferentiated stem cell fate in postnatal spermatogonia.

RESULTS

RB1 activity during prospermatogonial and postnatal spermatogonial development

RB1 is well known as a repressor of cell cycle progression in many cell types and its actions are inhibited by post-translational phosphorylation (Burke et al., 2012; Dick and Rubin, 2013). To explore the relationship of RB1 abundance as an active and inactive form and proliferation status of prospermatogonia, we used co-immunofluorescence staining for phosphorylated RB1 at serine residues 807/811 (designated p-RB1), a marker of active proliferation (Ki67) and the germ cell-specific marker TRA98 on cross-sections of testes from fetal and neonatal wild-type mice (Fig. 1). Co-staining revealed that RB1 is present in prospermatogonia and somatic cells throughout development, consistent with previous reports (Spiller et al., 2010; Western et al., 2008), but p-RB1 is detectable in prospermatogonia during the period of proliferation from E12.5 to E13.5 and becomes low to undetectable at E14.5-P1.5, which is coincident with the period of mitotic arrest. Thereafter, staining for p-RB1 increased by P6.5 when establishment of spermatogonial subsets, including the foundational SSC pool, occurs (Law et al., 2019). Taken together, these observations indicate that RB1 is active as a cell cycle repressor coincident with the period of mitotic arrest of prospermatogonia during late fetal and early neonatal development.

Inactivation of *Rb1* at the PGC stage results in male germline ablation

Previous studies showed that conditional inactivation of *Rb1* in prospermatogonia after the initiation of quiescence led to loss of the germline following one or two rounds of spermatogenesis in postnatal life, implying breakdown in the SSC pool (Hu et al., 2013; Yang et al., 2013). However, the ramifications of impaired cell cycle regulation caused by *Rb1* inactivation in prospermatogonia prior to initiation of quiescence during fetal development was not explored. To address this gap in knowledge, we used the Cre-Lox approach by backcrossing mice harboring *Rb1* floxed alleles and a *Blimp1-Cre* transgene to generate a model of conditional *Rb1* inactivation at the PGC stage, which is prior to prospermatogonial formation and the onset of quiescence, designated hereafter as *Rb1*-cKO^{Blimp1} (Fig. 2A). The *Blimp1-Cre* transgene is known to initiate expression starting at E6.5 and the efficiency of recombining floxed genes has been measured at >75% (Li et al., 2015; Ohinata et al., 2005). *Rb1*-cKO^{Blimp1} mice were born at the expected frequency and postnatal development was grossly normal with a lifespan that was similar to that of wild-type mice. As early as P14.5, testis weight of *Rb1*-cKO^{Blimp1} males was significantly ($P \leq 0.05$) reduced to 68.8% of that of control mice with one or two functionally intact *Rb1* alleles. (Fig. 2B), and these animals were sterile at all ages examined from P45 to P90 (Fig. 2C), demonstrating that, unlike males with conditional inactivation of *Rb1* in prospermatogonia after initiation of quiescence, even a first round of spermatogenesis does not occur. In accordance, assessment of testis cross-sections at P35, when the first round of spermatogenesis normally completes, and P60-180, when steady-state spermatogenesis has normally commenced,

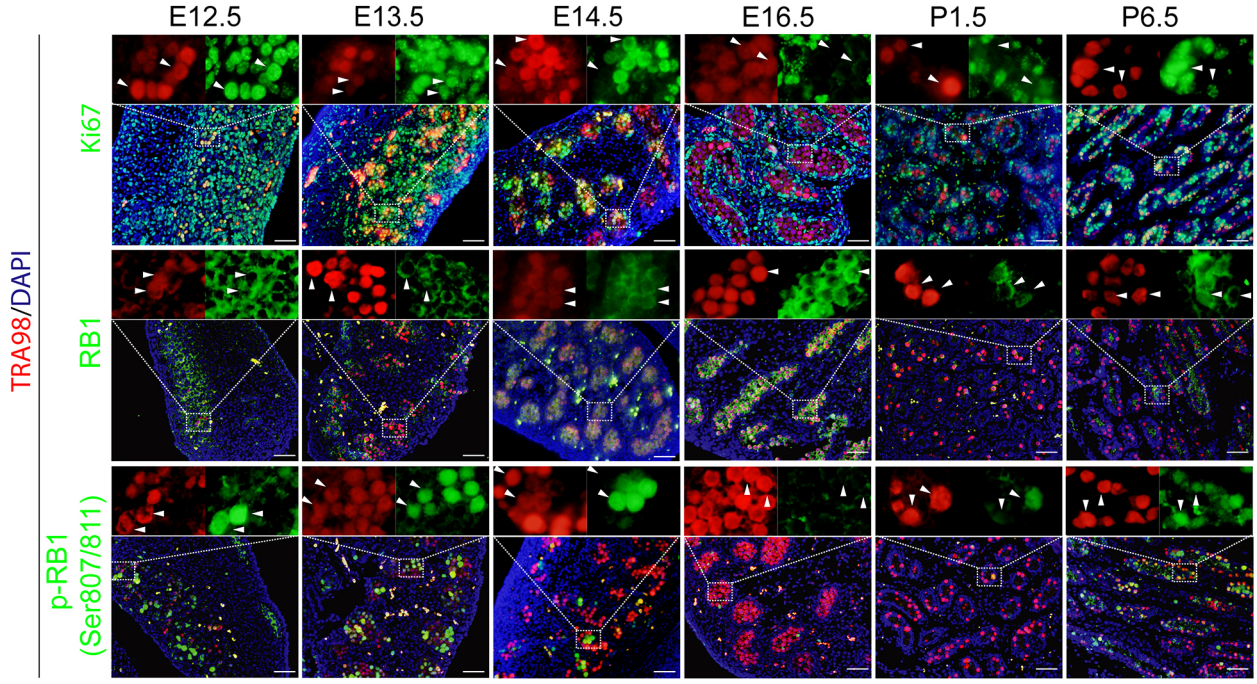

Fig. 1. Alignment of proliferation status with the active and phosphorylated inactive form of RB1 protein in male germ cells during fetal and neonatal development. Representative images of cross-sections from E12.5 to P6.5 mouse male gonads that were immunostained for the germ cell marker TRA98 (red) and proliferation marker Ki67 (green), total RB1 or phosphorylated RB1 [p-RB1(Ser807/811)]. Cell nuclei are labeled by DAPI staining (blue). Images are representative of testes from n=3 mice at each developmental age point. Scale bars: 50 µm.

Development (2021) 148, dev194571. doi:10.1242/dev.194571

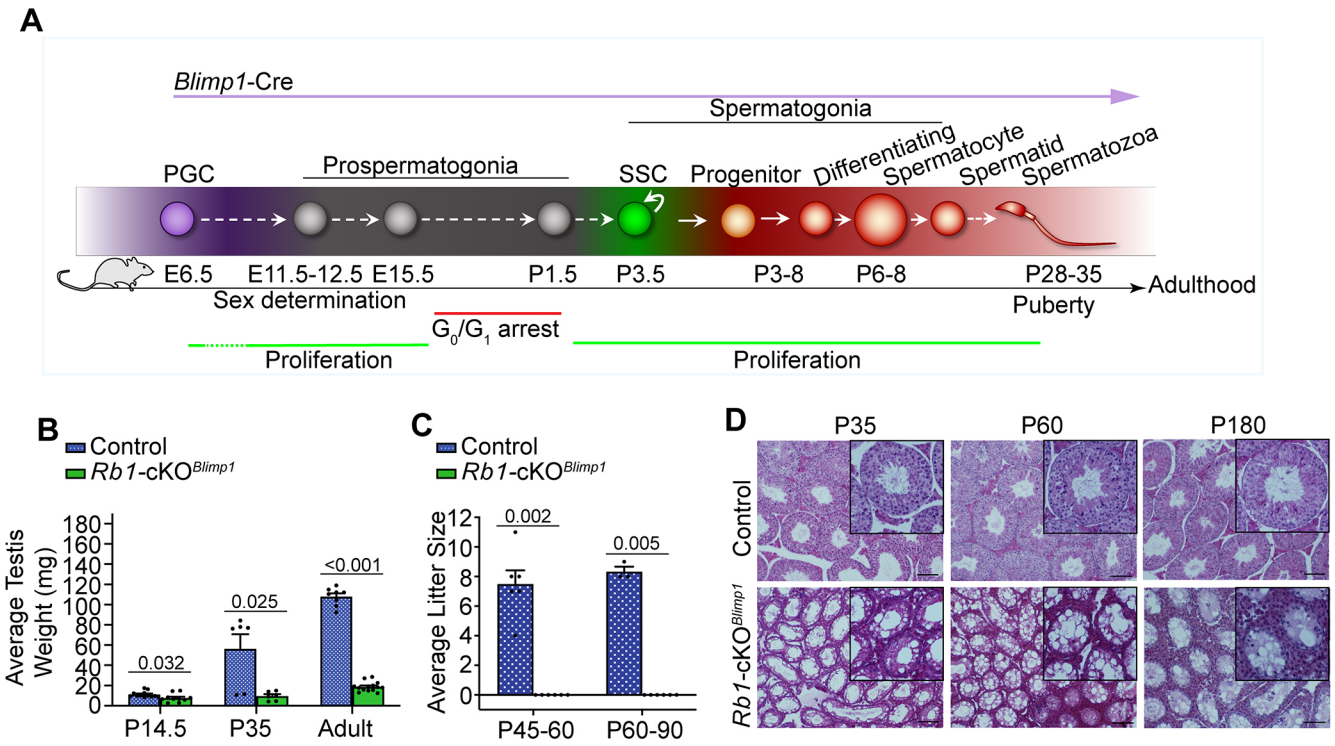

Fig. 2. Impacts of *Rb1* conditional inactivation in male primordial germ cells on establishment of the spermatogenic lineage. (A) Schematic overview of male germline development and when germ cell-specific *Rb1* conditional knockout (cKO) occurs in a mouse model using a Cre-Lox strategy with a *Blimp1-Cre* transgene. (B) Quantification of testis weights for control and *Rb1-cKO*^{Blimp1} mice at P14.5, P35 and adulthood. Data are mean±s.e.m. for *n*=6 (P14.5), 3 (P35) and 4 (adult) different males of each genotype and dots represent individual testes. (C) Assessment of fertility based on litter size for control and *Rb1-cKO*^{Blimp1} adult males at the ages P45-60 and P60-90 following mating with wild-type females. Data are mean±s.e.m. for *n*=3 different mice of each genotype. (D) Representative images of Hematoxylin and Eosin-stained cross-sections from testes of control and *Rb1-cKO*^{Blimp1} mice at P35, P60 and P180. Scale bars: 100 µm. Insets are magnifications of representative seminiferous tubules. For quantitative data comparisons in B and C, statistical analyses were performed with Mann–Whitney *U*-tests, and *P*-values are listed above comparisons with significant differences.

confirmed the cause of sterility as germline ablation in *Rb1*-cKO^{Blimp1} mice (Fig. 2D). In addition, body weights for *Rb1-cKO*^{Blimp1} mice were not different ($P\geq0.05$) to controls (Fig. S1A) and copulatory plugs were observed at all ages examined, confirming that mating had occurred. Furthermore, *Rb1-cKO*^{Blimp1} females were fertile well into adulthood despite significantly ($P\leq0.05$) smaller litter sizes compared with controls (Fig. S1B), similar to the phenotype of female mice with germline conditional inactivation of *Rb1* after sex determination, which may be accounted for by dysregulation of follicle growth (Yang et al., 2013, 2015), and/or uterine deficiencies (Goolam et al., 2020). Collectively, these findings suggest that proper cell cycle regulation during the prospermatogonial stage of development to ensure correct timing of mitotic arrest is crucial for establishment of the SSC pool and laying of the foundation for continuity of the spermatogenic lineage in postnatal life.

Disrupted entry into quiescence leads to apoptosis of prospermatogonia

In considering the phenotype of mice with conditional inactivation of *Rb1* either prior to or after onset of prospermatogonial quiescence, we were intrigued that disruption in the normal timing of mitotic arrest (i.e. *Rb1*-cKO^{Blimp1} males) led to germline ablation throughout all of postnatal life, but inactivation after initiation of quiescence (generated by backcrossing *Rb1-floxed* and *Ddx4-Cre* transgenic mice) did not disrupt the first round of spermatogenesis (Hu et al., 2013; Yang et al., 2013). These findings suggested that lack of RB1 per se does not impair prospermatogonial survival, but disruption of proper initiation of mitotic arrest is crucial. In global *Rb1*-null mice, germline development appears phenotypically normal up to E12.5 with the number of PGCs and prospermatogonia being unaltered, at which point embryonic death occurs (Spiller et al., 2010). We aimed to validate and extend these findings *in vivo* using *Rb1*-cKO^{Blimp1} males. In confirmation of previous results, both germ cell number and proliferation were found to be no different ($P\geq0.05$) between control and *Rb1*-cKO^{Blimp1} mice at E13.5 (Fig. S2A,B). However, based on positive immunostaining for the marker Ki67, 85.9% of prospermatogonia were found to be proliferating in *Rb1*-cKO^{Blimp1} mice at E14.5, which was significantly greater ($P\leq0.01$) compared with 59.1% of prospermatogonia in controls (Fig. 3A,B). This difference was even more striking at E16.5 when 65.2% of *Rb1*-cKO^{Blimp1} prospermatogonia were Ki67^{+} compared with 1.9% in control mice (Fig. 3A,B). By E18.5, the percentage of proliferating prospermatogonia in *Rb1*-cKO^{Blimp1} mice dropped to 4.9% but was still significantly greater ($P\leq0.05$) compared with control mice (Fig. 3A,B). These findings demonstrate that lack of *Rb1* altered the normal timing of mitotic arrest during fetal prospermatogonial development.

At E14.5, the number of prospermatogonia in *Rb1*-cKO^{Blimp1} mice was not different compared with the normal situation in control mice but, consistent with elevated proliferation, prospermatogonial number at E16.5 was significantly ($P\leq0.05$) greater in *Rb1*-cKO^{Blimp1} mice compared with controls (Fig. 3C). Thereafter, the number of prospermatogonia in both control and *Rb1*-cKO^{Blimp1} mice declined by E18.5, consistent with normal development, but the reduction in

Development (2021) 148, dev194571. doi:10.1242/dev.194571

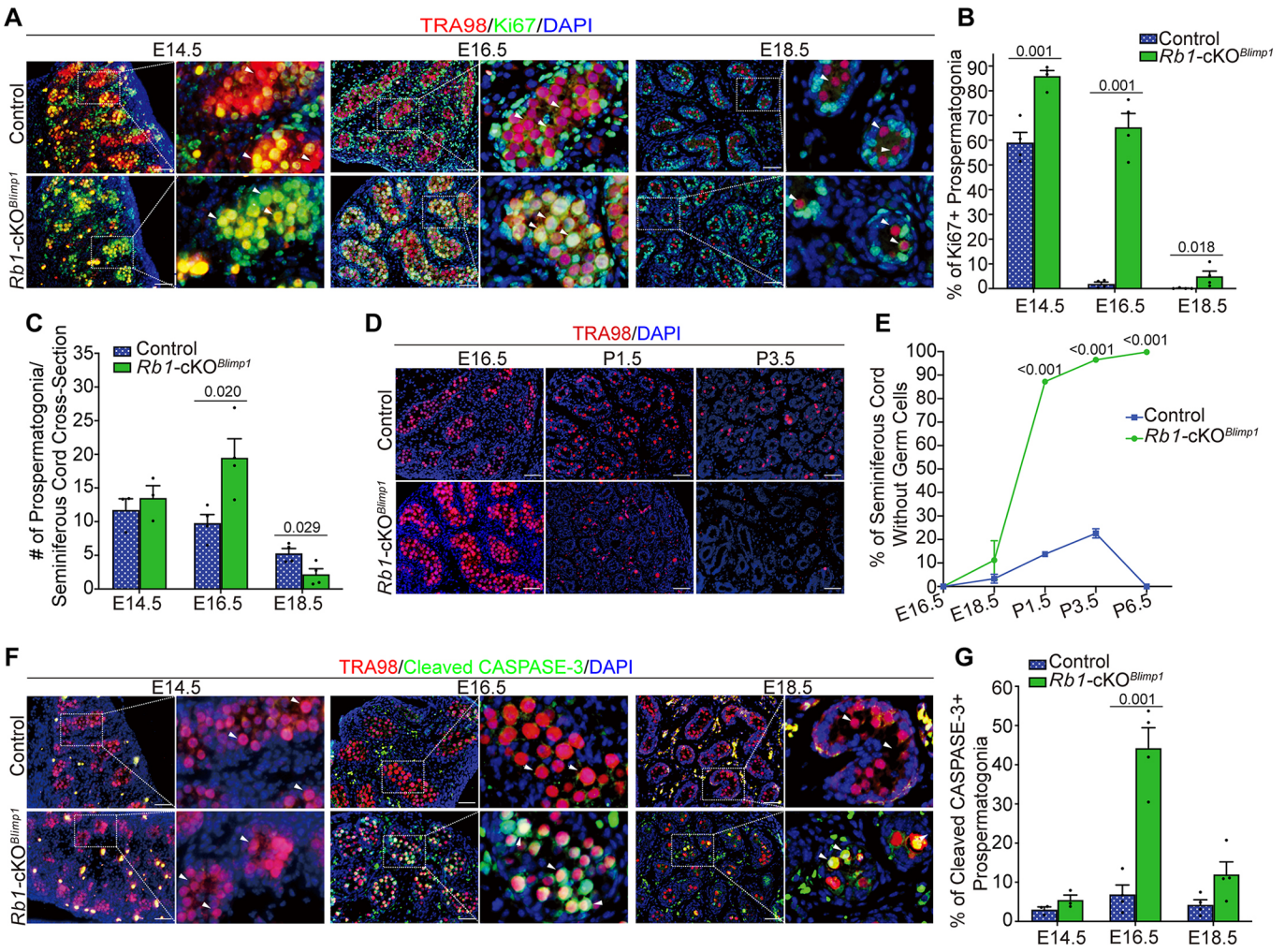

Fig. 3. Effects of disrupted entry into quiescence on prospermatogonial survival and function. (A,B) Representative images (A) and quantification (B) of immunofluorescence staining for expression of the proliferation marker Ki67 (green) in prospermatogonia of *Rb1-cKO*^{Blimp1} and control fetuses during the developmental time frame of E14.5-18.5 when quiescence normally occurs. (C) Quantification of prospermatogonial number per seminiferous cord cross-section in *Rb1-cKO*^{Blimp1} and control mice at E14.5-18.5. (D) Representative images of immunofluorescence staining for germ cells in cross-sections of seminiferous cords from *Rb1-cKO*^{Blimp1} and control mice at E16.5, P1.5 and P3.5. (E) Quantification of the percentage of seminiferous cord cross-sections lacking germ cells in control and *Rb1-cKO*^{Blimp1} mice at E16.5-P6.5. (F,G) Representative images (F) and quantification (G) of immunofluorescence staining for the apoptotic marker cleaved CASPASE-3 (green) in prospermatogonia of seminiferous cord cross-sections from control and *Rb1-cKO*^{Blimp1} fetuses at E14.5-18.5. For all images, germ cells were labeled as TRA98^{+}. Scale bars: 50 µm. For B, C, E and G, quantitative data are mean±s.e.m. from *n*=3-4 different mice of each genotype, dots represent values of individual animals, statistical analyses were performed using unpaired Student's *t*-tests, and *P*-values are listed above comparisons with significant differences.

Rb1-cKO^{Blimp1} was significantly ($P \leq 0.05$) greater compared with controls (Fig. 3C). Examination of testis cross-sections revealed that the percentage of seminiferous cords devoid of germ cells increased through developmental time in *Rb1*-cKO^{Blimp1} mice beginning with 11.2% at E18.5, jumping to 87.2% at birth (i.e. P1.5), and eventually leading to germline ablation (i.e. >95%) by P3.5-6.5 (Fig. 3D,E). In contrast, no cords lacked germ cells at P6.5 in control mice (Fig. 3D, E). Based on co-immunostaining for TRA98 and cleaved CASPASE-3, the level of germ cell apoptosis was not different ($P \geq 0.05$) between control and *Rb1*-cKO^{Blimp1} mice at E14.5 or E15.5 (Fig. 3F,G, Fig. S2C). However, by E16.5 44.2% of prospermatogonia were apoptotic in *Rb1*-cKO^{Blimp1} mice, which was significantly greater ($P \leq 0.05$) compared with the 6.9% of prospermatogonia undergoing apoptosis in control mice (Fig. 3F,G). Collectively, these findings indicate that failure of prospermatogonia to enter quiescence on a normal developmental timeline leads to programmed cell death.

scRNA-seq defines alterations in the transcriptome of *Rb1*-deficient prospermatogonia

Considering that RB1 has diverse cellular functions beyond regulation of cell cycle progression, we next aimed to explore whether additional mechanisms underpin the impaired survival of prospermatogonia in *Rb1*-cKO^{Blimp1} males. To achieve this, we performed scRNA-seq on E14.5 testes, which was the developmental age point when interruption of the normal entry point to quiescence occurred and apoptosis was not different between *Rb1-cKO* and control prospermatogonia (Fig. 3A,B,F,G), thus allowing for assessment of the root causes of impaired programming due to *Rb1* deficiency rather than ramifications that would manifest later in development. To focus the analysis on prospermatogonia, we generated a multi-transgenic mouse model in which simultaneous inactivation of *Rb1* and constitutive activation of *tdTomato* expression occurs in all PGCs (Fig. S3A). Prospermatogonia from E14.5 *Rb1*-cKO^{Blimp1}*;tdTomato*$^{+}$ (n=3) and control (*Blimp1*-Cre$^{Tg/+}$;

Development (2021) 148, dev194571. doi:10.1242/dev.194571

Rb1$^{fl/+}$;*tdTomato*$^{+}$, *n*=3) mice were isolated by fluorescence-activated cell sorting (FACS) and single-cell mRNA libraries generated with the 10x Genomics platform followed by Illumina sequencing analysis. Notably, *Rb1* transcripts were undetectable in all libraries generated for *Rb1*-cKO^{Blimp1} prospermatogonia (Fig. S3B), thus demonstrating complete penetrance of the Cre-Lox approach. In addition, consistent with findings of Spiller et al. (2010) that examined *Rb1* null prospermatogonia, expression of the *Rb1* family members *p107* (*Rbl1*) and *p130* (*Rbl2*) in *Rb1-cKO* prospermatogonia was not different compared with *Rb1*-sufficient control prospermatogonia (Fig. S3B).

A total of 3560 and 4025 cells were captured from control and *Rb1*-cKO^{Blimp1};*tdTomato*$^{+}$ males, respectively (Fig. S3B,C). Transcriptomes were sequenced at an average depth of 49,332 and 41,976 reads per cell representing an average sequencing saturation of 51% and 54% for control and *Rb1*-cKO^{Blimp1};*tdTomato*$^{+}$, respectively. Averages of 17,149 and 17,237 genes were detected across pooled triplicate libraries for control and *Rb1*-cKO^{Blimp1};*tdTomato*$^{+}$ samples, respectively. Single-cell transcriptomes were then filtered based on quality control metrics (Fig. S3D,E), including selection for those with <300 genes detected to remove low-quality transcriptomes and >6.5% mitochondrial gene representation to remove dead cells, and exclusion of transcriptomes with >50,000 genes to remove potential doublets. Germ cells in each library were then defined based on expression of well-known specific marker genes, such as *Ddx4* (Gallardo et al., 2007), *Dazl* (Nicholas et al., 2009) and *Pou5f1* (Yoshimizu et al., 1999) (Fig. S3F). After filtering, a total of 5160 germ cells were analyzed further (2568 and 2592 in control and in *Rb1*-cKO^{Blimp1};*tdTomato*$^{+}$, respectively).

scRNA-seq analysis revealed highly consistent transcriptomic signatures of triplicate samples based on modified Pearson's correlation coefficients of 0.988-0.996 among control libraries and 0.990-0.995 among *Rb1*-cKO^{Blimp1};*tdTomato*$^{+}$ libraries. Based on the results above, which demonstrated the central role of *Rb1* in cell cycle arrest *in vivo*, we first investigated whether gene expression profiles from scRNA-seq reflected *in vivo* measurements. To do so, CellCycleScoring analysis was performed between control and *Rb1*-cKO^{Blimp1} samples, which predicted cell cycle phase based on relative gene expression signatures. This analysis revealed that a significantly greater ($P \leq 0.05$) proportion of prospermatogonia were in S/G_2/M in *Rb1*-cKO^{Blimp1};*tdTomato*$^{+}$ males compared with controls (Fig. 4A). The expression of *Ki67* is generally upregulated across S/G_2/M (Miller et al., 2018); thus, cell cycle predictions from scRNA-seq are consistent with the *in vivo* Ki67 staining (Fig. 3).

Owing to the asynchronous nature of germ cell development and heterogeneity of gene expression in wild-type cells at the embryonic/fetal age points of E12.5-18.5 (Law et al., 2019; Nguyen et al., 2019, 2020), we first aimed to explore whether disruption of entry to mitotic arrest on a normal timeline alters transcriptome profiles throughout the prospermatogonial population.

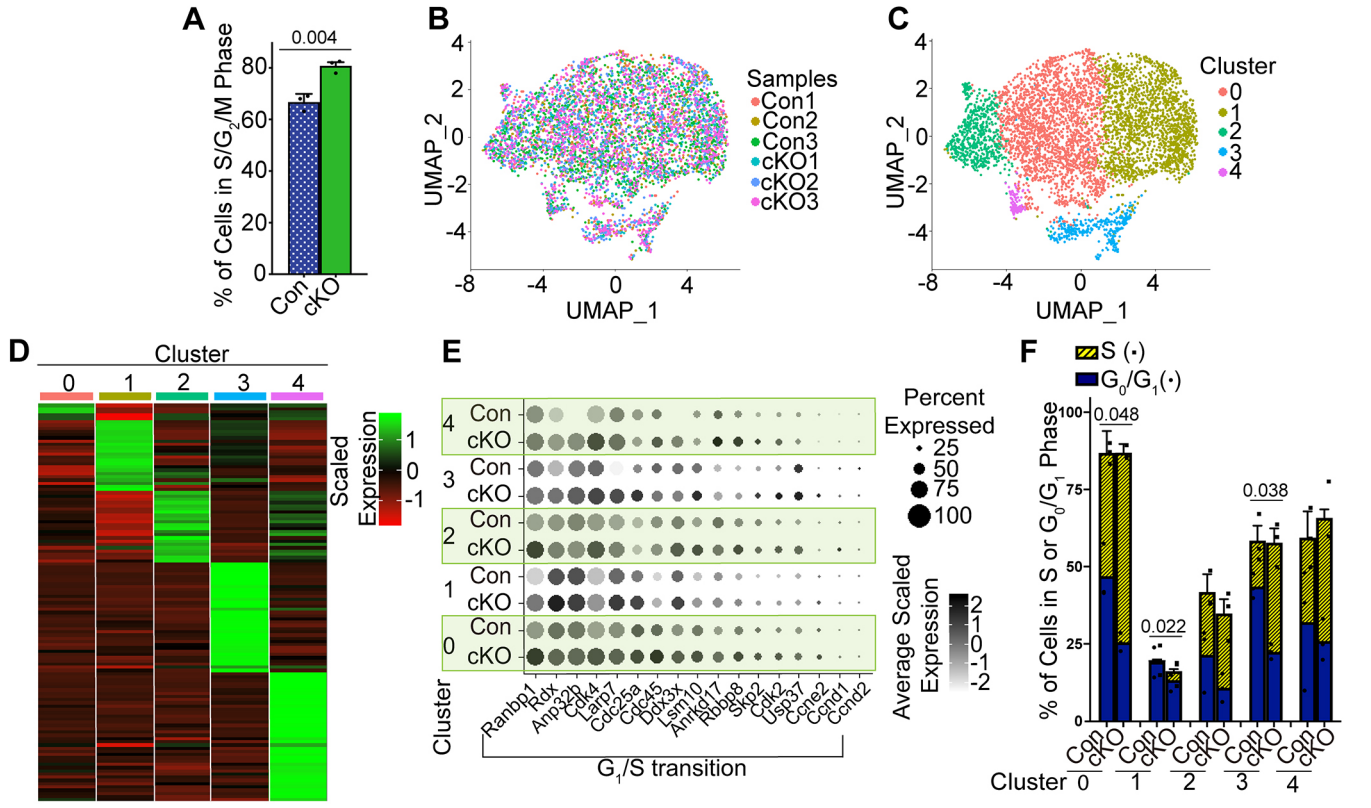

Fig. 4. Impacts of impaired cell cycle regulation on the transcriptome in prospermatogonia at a single-cell resolution. (A) Percentage of prospermatogonia in control or *Rb1-cKO*^{Blimp1} mice determined to be in S/G_2/M phase of the cell cycle based on CellCycleScoring analysis from scRNA-seq transcriptome profiles. (B,C) UMAP representation of individual libraries (B) and graph-based clusters (C) for prospermatogonia isolated from control or *Rb1-cKO*^{Blimp1} mice. (D) Heatmap of the top 130 marker genes for each cluster distributed in C. (E) Dot plot representation of average scaled expression (color gradient) and the percentage of cells in each UMAP-defined cluster with detectable expression (dot size) for genes associated with the G_1/S transition. (F) Quantitative assessment of the percentage of prospermatogonia in different UMAP-defined clusters for control and *Rb1-cKO*^{Blimp1} mice at E14.5 that were determined to be in G_0/G_1 or S phases of the cell cycle using CellCycleScoring analysis. For A and F, quantitative data are mean±s.e.m. for *n*=3 different mice of each genotype, dots represent data points of individual mice, statistical analyses were performed using unpaired Student's *t*-tests, and *P*-values are listed above comparisons with significant differences.

Development (2021) 148, dev194571. doi:10.1242/dev.194571

Using a method of comprehensive integration, we aligned the six libraries followed by uniform manifold approximation projection (UMAP) and graph-based clustering to capture germ cell heterogeneity at E14.5 (Fig. 4B,C). A total of five clusters were identified using shared nearest neighbor modularity optimization with a resolution of 0.2. Under this resolution, clusters were well-distinguished from each other based on differential gene expression (Fig. 4D; gene list in Table S1). Annotation of marker genes suggested that clustering was influenced by cell cycle phase. For example, *Ccne1* and *Rrm2*, upregulated in cluster 0, function in the G_1/S transition (DeGregori et al., 1995), and *Ube2c* and *Ube2s*, upregulated in cluster 1, promote mitotic exit (Sivakumar and Gorbsky, 2015) (Fig. S3G). Consistent with differential gene expression analysis, CellCycleScoring predicted that 38.0% and 48.9% of germ cells in cluster 0 were in phases G_0/G_1 and S, respectively, whereas the cells in the cluster 2 were primarily in G_2/M (Fig. S3H). Taken together, clustering effectively defined germ cell heterogeneity such that differences between control and cKO would not be masked by population diversity.

Using the clustering approach described above, we then defined differentially expressed genes (DEGs) between control and *Rb1*-cKO^{Blimp1};*tdTomato*$^{+}$ males in the context of germ cell heterogeneity (see gene list in Table S2). Transcripts associated with cell cycle regulation were among the top Gene Ontology (GO) terms in clusters 0, 1, 2 and 3 (based on $P \leq 0.01$) (Table 1). In particular, genes associated with promotion of the G_1/S transition were upregulated in *Rb1*-cKO^{Blimp1};*tdTomato*$^{+}$ within each of the clusters (Fig. 4E). As a result, a greater proportion of germ cells transitioned from G_0/G_1 to S phase with *Rb1* inactivation across all clusters based on CellCycleScoring (Fig. 4F). Collectively, these data indicate that prospermatogonia arrest in G_0/G_1 and in the absence of RB1 the G_1/S checkpoint is bypassed leading to an inability for entry into mitotic arrest on a normal timeline.

Mitotic arrest aligns with a metabolic shift and meiotic inhibition in prospermatogonia

Collectively, the phenotypic impacts of delaying entry to mitotic arrest by conditionally inactivating *Rb1* in the developing male germline suggested that a period of proliferative quiescence is important during the prospermatogonial stage to program fate commitment in postnatal development. To explore this critical time further, we first sought to construct a temporal map of cellular processes that occur in normal prospermatogonia during mitotic arrest. Using this map, we then cross-referenced perturbations that occurred when *Rb1* was inactivated to identify cellular functions that may be dependent on mitotic arrest.

To build a developmental trajectory of prospermatogonia, we first integrated publicly available scRNA-seq datasets from isolated prospermatogonia spanning from E12.5 to SSC establishment at P3.5 (GEO accession numbers GSE119045 and GSE124904; Fig. 5A,B). Because of the asynchronous nature of germline development, single-cell transcriptomes were ordered using pseudotime analysis in Monocle, which accurately places the trajectory analyses with respect to developmental ages. Next, we performed differential gene expression analysis through pseudotime and identified six broad groups with distinct gene expression patterns (Fig. 5C, gene list located in Table S1). The expression of genes associated with cell cycle regulation (Group 2, Fig. 5C,D)

Table 1. Top 5 gene ontology classifications based on up- or downregulated genes from scRNA-seq analysis of control and *Rb1-cKO*^{Blimp1} mice at E14.5

GO terms upregulated	*P*-value	GO terms downregulated	*P*-value
Cluster 0			
Cell cycle	2.63E−35	Translation	8.71E−14
DNA repair	3.67E−22	Transcription from RNA polymerase II promoter	6.23E−05
Cellular response to DNA damage stimulus	3.37E−21	rRNA processing	7.04E−05
DNA replication	3.96E−21	mRNA processing	8.57E−05
Cell division	5.20E−20	Oxidation-reduction process	1.25E−04
Cluster 1			
Cell cycle	3.52E−26	Translation	4.54E−18
Cellular response to DNA damage stimulus	2.52E−21	mRNA processing	5.36E−07
DNA replication	6.32E−21	Oxidation-reduction process	4.32E−06
DNA repair	4.27E−20	ATP synthesis coupled proton transport	1.04E−05
mRNA processing	2.58E−17	Proton transport	3.37E−05
Cluster 2			
Cell cycle	1.37E−19	Translation	4.97E−24
mRNA processing	7.71E−15	Cytoplasmic translation	4.62E−08
RNA splicing	3.77E−13	Hydrogen ion transmembrane transport	9.03E−07
Protein folding	1.84E−12	ATP synthesis coupled proton transport	3.95E−06
Cell division	9.45E−11	Proton transport	9.48E−06
Cluster 3			
Cell cycle	3.00E−11	Translation	1.49E−04
Cellular response to DNA damage stimulus	3.44E−09	Negative regulation of proteasomal protein catabolic process	0.0030796
DNA repair	1.09E−08	Protein transport	0.0071188
DNA recombination	4.63E−08	Positive regulation of glucose import	0.0077828
Cell division	3.03E−06	Mitochondrial respiratory chain complex IV assembly	0.0126045
Cluster 4			
Transcription, DNA-templated	6.79E−05	Ribosomal large subunit assembly	3.48E−04
DNA repair	1.71E−04	Transcription, DNA-templated	4.59E−04
mRNA transport	2.40E−04	Apoptotic process	0.0014835
Cellular response to DNA damage stimulus	3.10E−04	Cellular response to hypoxia	0.0024130
Regulation of transcription, DNA-templated	4.66E−04	Cell cycle	0.0032502

Development (2021) 148, dev194571. doi:10.1242/dev.194571

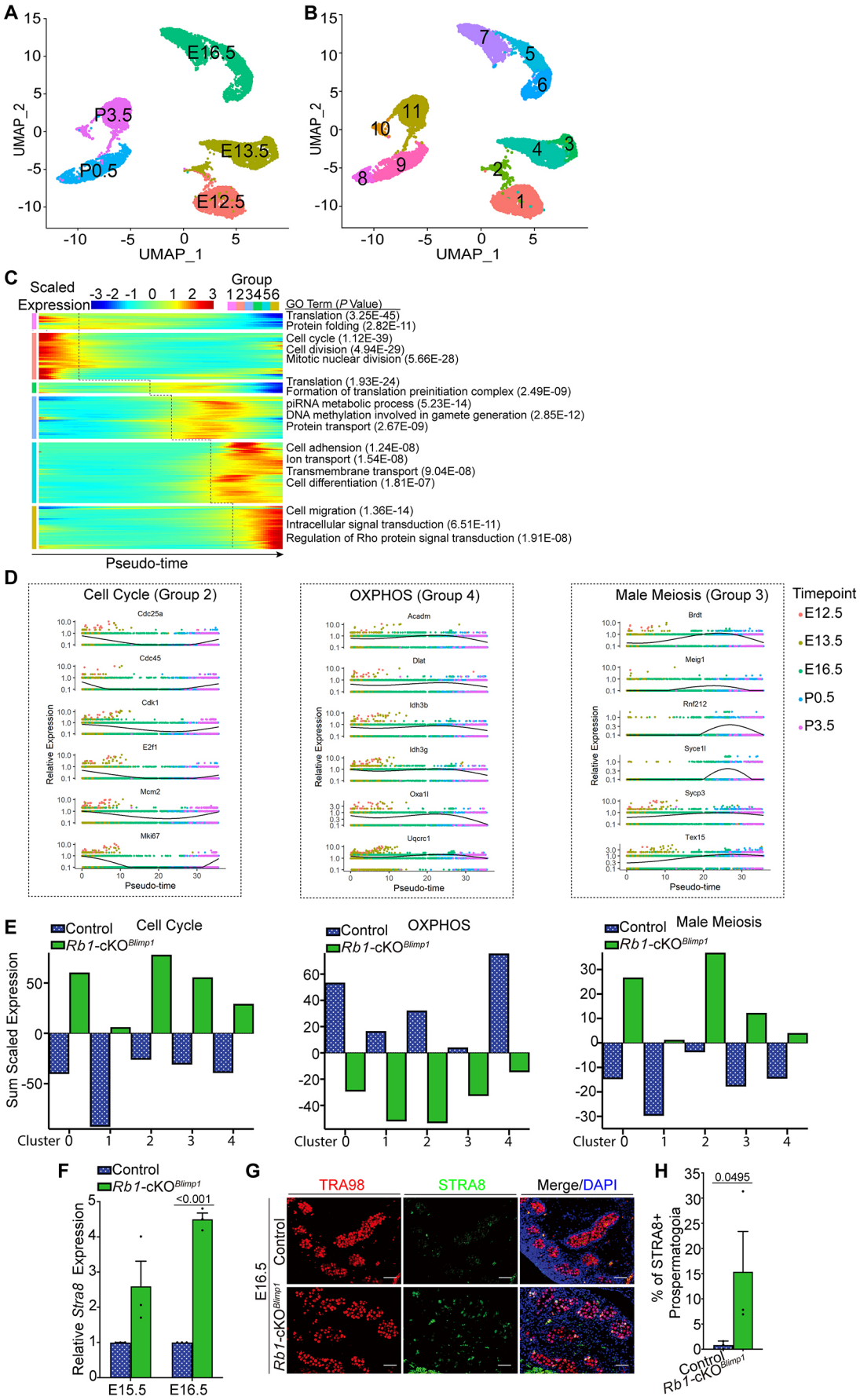

Fig. 5. See next page for legend.

Development (2021) 148, dev194571. doi:10.1242/dev.194571

Fig. 5. Assessment of changing cellular processes during the quiescent period in prospermatogonia. (A,B) UMAP representations of scRNA-seq transcriptome profiles for germ cells isolated from testes of mice at E12.5-P3.5. (C) Heatmap representation of differential gene expression in six cellular groupings through pseudotime and binned as GO terms. The number of genes represented in groups 1-6 is 766, 2210, 2005, 496, 2871 and 2021, respectively. (D) Temporal expression of genes associated with positive cell cycle progression, OXPHOS and male meiosis along the normal developmental trajectory in mice organized as pseudotime. (E) Sum of scaled DEGs that regulate positive cell cycle progression, OXPHOS and male meiosis in prospermatogonial clusters (defined by scRNA-seq analysis) of control and *Rb1-cKO*^{Blimp1} mice at E14.5. (F) Comparison of relative *Stra8* mRNA abundance in embryonic testes of control and *Rb1-cKO*^{Blimp1} mice at E15.5 and E16.5. Data were generated from qRT-PCR analysis and are mean±s.e.m. for n=3 different mice of each genotype. Dots represent data points of individual mice, statistical analyses were performed using unpaired Student's *t*-tests, and *P*-values are listed above comparisons with significant differences. (G,H) Representative images (G) and quantification (H) of immunofluorescence staining for TRA98^{+} germ cells (red) and the meiotic marker STRA8 expression (green) in cross-sections of testes from control and *Rb1-cKO*^{Blimp1} mice at E16.5. Cell nuclei are labeled with DAPI (blue). Scale bars: 50 µm. Quantitative data in H are mean±s.e.m. for n=3 different mice of each genotype, dots represent data points of individual mice, statistical analyses were performed using a Mann–Whitney *U*-test, and *P*-values are listed above comparisons with significant differences.

declined early along the trajectory and were upregulated towards the end, consistent with the cell cycle progression of prospermatogonia *in vivo*. In addition, well-described processes, such as DNA methylation (Group 3), piRNA metabolism (Group 3) and cell migration (Group 6) were temporally regulated along the trajectory in a manner consistent with *in vivo* progression (Fig. S4). Collectively, our pseudotime analysis accurately recapitulated the *in vivo* germ cell developmental trajectory.

Interestingly, we also identified indications of metabolic shifts along the germ cell trajectory (Group 4, Fig. 5C,D). Genes associated with oxidative phosphorylation (OXPHOS) transiently increased in expression among quiescent prospermatogonia before decreasing during the period of cell cycle re-entry. To begin to assess whether metabolic shifts are disrupted in prospermatogonia that do not initiate mitotic arrest on a normal timeline, we applied filtering to the scRNA-seq database of E14.5 *Rb1*-cKO^{Blimp1} and control prospermatogonia to standardize for the percentage of mitochondrial gene expression (Table S3), thereby allowing for focused assessment on nuclear-derived OXPHOS-related mRNAs. With cell cycle progression being disrupted in *Rb1*-cKO prospermatogonia (Fig. 5E, Fig. S5A and gene list in Table S1), genes associated with OXPHOS were also significantly downregulated across the entire population at E14.5 compared with controls (Fig. 5E, Figs S5B, S6A, and gene list in Table S1). These findings indicate that the normal transition to OXPHOS is influenced by cell cycle arrest, although additional biochemical experimentation is needed to fully support this concept. In addition, expression of genes that drive glycolysis, such as *Eno1*, were found to be upregulated in *Rb1*-cKO prospermatogonia compared with *Rb1*-sufficient control cells (Fig. S7), thus further supporting the notion of altered OXPHOS activity.

Surprisingly, expression of genes associated with male meiosis were not only detected along the germ cell developmental trajectory in wild-type mice, but also transiently upregulated around E16.5 (Fig. 5D). This observation is unexpected given that male germ cells enter meiosis postnatally unless misplaced outside seminiferous cords during fetal development (Zamboni and Merchant, 1973). However, with *Rb1* inactivation, the expression of genes associated with male meiosis were upregulated at E14.5 (Fig. 5E, Figs S5C, S6B, and gene list in Table S1) and no indications of aberrant germ cell colonization were observed (Fig. 3). To assess the ramifications of disrupted entry into quiescence on a normal timeline that should have occurred at E14.5 *in vivo*, we assayed for transcript abundance and protein expression for the meiotic marker gene *Stra8* (Zhou et al., 2008) in testes of *Rb1*-cKO^{Blimp1} mice at E16.5. The relative abundance of *Stra8* transcripts at E16.5 was significantly higher ($P \leq 0.05$) in *Rb1*-cKO prospermatogonia compared with controls (Fig. 5F). Strikingly, immunostaining of testis cross-sections revealed a significant ($P \leq 0.05$) increase by ∼18-fold in the percentage of STRA8^{+} prospermatogonia in *Rb1*-cKO^{Blimp1} testes at E16.5 compared with controls (Fig. 5G,H), and by E18.5 the leveled increase in *Rb1-cKO* cells had dropped by ∼50% but was still greater compared with controls (Fig. S7A,B). The ectopic expression of STRA8 and significant increase in expression of genes related to meiosis indicate that inhibition of meiotic entry could be compromised in *Rb1*-cKO prospermatogonia. Overall, these findings suggest that the period of mitotic arrest in prospermatogonia facilitates a metabolic shift to an OXPHOS state and inhibition of meiotic initiation, which likely influence or accompany proper establishment of the SSC pool in postnatal development (Fig. 6).

DISCUSSION

Although a period of mitotic arrest and then re-initiation of cell cycle progression in prospermatogonia are events known to occur during genesis of the male germline, the underlying regulatory mechanisms driving these steps and the functional importance of this were not known. Here, and in previous studies (Yang et al., 2013), we developed mouse models to address these gaps in knowledge by eliminating the master cell cycle regulator RB1 in prospermatogonia prior to the normal timing of when entry and exit of mitotic arrest should occur. Previous studies have established that the prospermatogonial population is heterogeneous with subsets possessing characteristic transcriptome profiles that are linked with functional fates to either form the foundational SSC pool or transition to a differentiating state directly (Kluin and de Rooij,

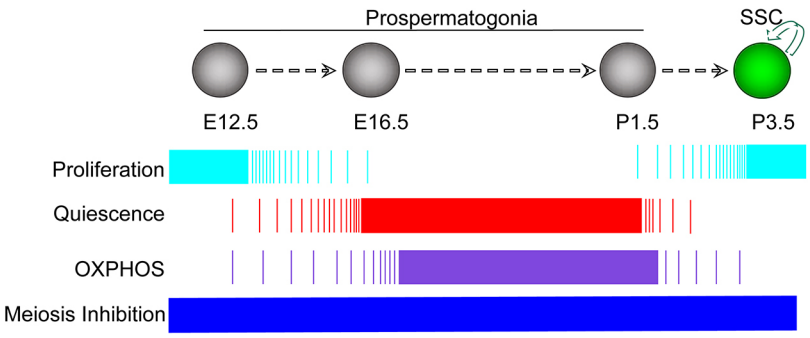

Fig. 6. Model of key cellular programming events that occur during the quiescent period in prospermatogonia. Proper timing of mitotic arrest during fetal development facilitates a metabolic shift to an OXPHOS state and prevents meiotic initiation. These events are essential for the generation of a prospermatogonial population that will serve as precursors of the spermatogenic lineage in postnatal life, including establishment of a foundational SSC pool.

Development (2021) 148, dev194571. doi:10.1242/dev.194571

1981; Law et al., 2019). In prospermatogonia lacking *Rb1* at the onset of their formation, entry into quiescence fails to occur on a normal timeline, thus leading to apoptosis of all subsets and subsequent germline ablation (findings from the present study). In contrast, when the prospermatogonial population enters quiescence on a normal time frame but re-initiation of cell cycle progression is disrupted, only the SSC pool fails to develop (Hu et al., 2013; Yang et al., 2013), thus suggesting that proper timing of mitotic re-entry is crucial for locking in SSC fate within prospermatogonia. Interestingly, we found that the prospermatogonial population still undergoes mitotic arrest even in the absence of RB1 activity but on a delayed time frame (E18.5) compared with the normal situation (E16.5), potentially due to compensatory activity of other cell cycle regulators, such as cyclin D, *Cdk4/6*, *Cdkn2a* and *Cdkn2b.* Regardless, the delay in timing of mitotic arrest leads to prospermatogonial apoptosis, which effectively ablates the germline in males. Thus, the act of entering mitotic arrest and doing so at the proper time in development are crucial factors in genesis of the spermatogenic lineage.

A wave of apoptosis in the prospermatogonial population is known to occur during perinatal development and has been speculated to eliminate aberrant cells (Bejarano et al., 2018; Nguyen et al., 2019; Wang et al., 1998). Indeed, recent studies demonstrated that prospermatognia with developmentally defective genetic and epigenetic integrity are eliminated by apoptosis in the mouse (Nguyen et al., 2020). Based on results of the current study that showed massive apoptosis of prospermatogonia lacking RB1 activity and therefore abnormal cell cycle regulation during fetal development, we speculate that correct timing of mitotic arrest is an indicator of proper fitness that saves cells from apoptosis and disruption of this timing leads to elimination of cells that would normally contribute to the spermatogenic lineage in postnatal life.

Proper cell cycle regulation is paramount to the development and continuity of all cellular lineages that support homeostasis. The germ cell lineage is the eternal link between generations and in males the genesis relies on proper transition between PGC, prospermatogonial and SSC states. Using mouse models, previous studies have tracked the proliferation kinetics and cell cycle status underlying the PGC stage of development. Around E6.25, PGC fate is initiated in a subset of epiblast cells (~40 precursor cells) that rapidly proliferate to ~25,000 cells by E13.5 (Tam and Snow, 1981), and full germ cell commitment is locked in after migration to the genital ridge has completed (Nicholls et al., 2019). Thus, it is interesting that PGCs develop normally in *Rb1*-cKO^{Blimp1} males, particularly when considering that proliferation rates among this population from E6.25 to E13.5 are not constant. Specifically, PGCs arrest in G_2 from E7.5 to E9.5 (Seki et al., 2007), and, based on gene expression profiles, cell cycle regulation closely resembles that of embryonic stem cells (ESCs) at E11.5, except for strict regulation of the G_1 phase (Sorrentino et al., 2007). ESCs lack a G_1/S checkpoint and can enter S phase rapidly following the previous M phase, and although *Rb1* is expressed by ESCs, the related pathway is not active (LeCouter et al., 1996; Rohwedel et al., 1996). Similar regulation appears to occur among PGCs from E9.5 onward, such that cell cycle progression is regulated independently of RB1 and is collectively more ESC-like. Consistent with this notion, we found that RB1 is hyperphosphorylated and inactive among germ cells from E12.5 to E13.5, but as germ cells enter mitotic arrest RB1 becomes a central regulator of quiescence.

In previous studies, we discovered that inactivation of *Rb1* in prospermatogonia of mice during the normal fetal quiescence period did not disrupt the first round of spermatogenesis in postnatal life, but the germline was summarily lost when subsequent rounds should commence (Hu et al., 2013; Yang et al., 2013). This phenotype implies that the foundational SSC pool required to regenerate the spermatogenic lineage following a round of differentiation was lacking. This observation begs the question of why the prospermatogonial subset normally fated to give rise to SSCs does not do so in the absence of RB1 to regulate cell cycle progression. Our recent studies indicate that prospermatogonia programmed during the quiescent period to adopt an SSC fate re-initiate cell cycle progression in neonatal development prior to the subset that is fated to initiate differentiation directly (Law et al., 2019). Thus, it is possible that inactivating *Rb1* and disrupting the timing of cell cycle re-entry led to apoptosis of the SSC-fated prospermatogonial subset or a differentiating fate was induced directly in these cells. An intriguing alternative possibility is that prospermatogonia normally fated in late fetal development to form the foundational SSC pool instead adopted a progenitor fate directly in neonatal development and therefore did not either contribute to the first round of spermatogenesis or function as stem cells to support continual spermatogenesis. This notion is supported by our recent predictions, built from scRNA-seq profiles of prospermatogonial subsets, which suggest the existence of at least three different prospermatogonial fate trajectories during neonatal development that are programmed during the fetal period (Law et al., 2019). It is possible that activation of the programming laid down during fetal development is intimately linked with the timing of cell cycle re-entry in the neonatal period; exploring this possibility will require future experimentation.

A major unanswered question in the field of male germ cell biology has been what occurs within prospermatogonia during the quiescent period? To address this and define how disrupted entry compromises prospermatogonial survival, we compared transcriptome profiles from cells with and without RB1 activity at E14.5. Thus, we were able to compare gene expression profiles in prospermatogonia that had initiated quiescence on a normal developmental timeline and prospermatogonia that had not entered quiescence at the same point in development. Interestingly, pathway analysis uncovered that genes associated with meiosis were upregulated and genes associated with OXPHOS were downregulated in RB1-deficient prospermatogonia. These findings suggest that inhibition of meiotic initiation and a shift in metabolic activity normally occurs in prospermatogonia during the quiescent period. However, additional experimentation with biochemical assays are needed to fully assess metabolic shifts during prospermatogonial development. Considering the relatively large number of cells that are needed to carry out metabolomic analyses, exploring changes in OXPHOS activity throughout developmental time in more depth will require future technological advances.

In corroboration of altered expression of meiosis-associated genes, a significantly greater proportion of prospermatogonia immunostained for the meiotic marker STRA8 in *Rb1*-cKO mice compared with controls at E16.5. Previous studies have reported a similar relationship between mitotic arrest and meiotic inhibition in spermatogonia that are deficient for the transcription factor BNC2 (Vanhoutteghem et al., 2014), suggesting that the two forms of cell division are tightly coupled in the germline.

Metabolism is known to be a driver of cellular bioenergetics but is also associated with regulation of cell signaling and the epigenome (Folmes et al., 2012). Indeed, plasticity in metabolic pathways allows stem cells to meet the divergent demands of self-renewal and differentiation. Also, ensuring a glycolytic state facilitates the induction and maintenance of pluripotency in induced pluripotent stem cells and ESCs (Folmes et al., 2012). In

Development (2021) 148, dev194571. doi:10.1242/dev.194571

addition, glycolysis is the primary bioenergetic process in SSCs and impacts their regenerative capacity (Chan et al., 2014; Helsel et al., 2017; Lord and Nixon, 2020). Furthermore, evidence from studies with embryonal carcinoma cells indicate that activation of OXPHOS activity triggers loss of pluripotency and transition to a differentiating state (Vega-Naredo et al., 2014). In addition, increased OXPHOS activity has been reported to occur during both PGC and SSC differentiation (Guo et al., 2017; Hayashi et al., 2017; Lord and Nixon, 2020; Varuzhanyan et al., 2019). Thus, metabolic shifts between functional states occur in many cell types but the mechanisms underpinning the process are largely unknown. Here, we found that in prospermatogonia when initiation of the quiescent period is disrupted by Rb1 inactivation, altered expression of genes associated with OXPHOS activity also occurs. This finding suggests that, similar to other types of stem cells, changing states of development align with a metabolic shift.

Features of germline development are highly conserved among mammals, and stringent maintenance of genetic integrity is crucial for proper inheritance regardless of species (Barton et al., 2016; Hamer and de Rooij, 2018; Murphey et al., 2013). During germ cell development, apoptosis that occurs at both fetal and postnatal ages is believed to select for the most robust cells to persist into adulthood and generate gametes that will pass genetic information to the next generation (Bejarano et al., 2018; Nguyen et al., 2020; Wang et al., 1998). The mechanisms for biosensing of germ cell fitness are largely unknown, but apoptosis is generally required to maintain reproductive fitness through the removal of developmentally incompetent or 'undesirable' cells, thereby ultimately ensuring maintenance of gamete quality (Aitken et al., 2011; Nguyen et al., 2020; Runyan et al., 2006). In the current study, we discovered that disruption of the normal developmental timing of when prospermatogonia enter quiescence leads to apoptosis and complete germline ablation. We postulate that, in addition to meiotic inhibition and metabolic shift, there are likely other key layers of programming being laid down during the quiescent period in prospermatogonia to ensure proper fate specification and fitness in postnatal life, and an ingrained biosensing mechanism eliminates cells that fail to initiate mitotic arrest on a correct developmental timeline.

MATERIALS AND METHODS

Animals

Mice were maintained under specific pathogen-free (SPF) conditions at 20-26°C and 40-70% humidity in the animal core of Washington State University. All animal procedures were approved by the Washington State University Institutional Animal Care and Use Committee (IACUC). *Rb1*^{flox} (*Rb1*^{fl}; stock #026563), *Blimp1-Cre* (*Blimp1-Cre*^{Tg}; stock #008827) and *Rosa26-tdTomato*$^{fl\_STOP\_fl}$ (stock #007909) transgenic mice were obtained from Jackson Laboratories. Primer sequences for genotyping have been previously described or are presented in Table S4. The day of mating plug detection was designated as E0.5 and the first day following birth was designated as P0.5.

To generate *Rb1*-cKO models, *Rb1*$^{fl/fl}$ female mice were first crossed with *Blimp1-Cre* male mice to obtain *Cre*^{Tg};*Rb*$^{fl/+}$ males that were then crossed with *Rb1*$^{fl/fl}$ females to obtain *Cre*^{Tg}; *Rb1*$^{fl/-}$ (*Rb1*-cKO). To generate multi-transgenic *Rb1* cKO males, *Rb1*$^{fl/fl}$;*Rosa26-tdTomato*$^{fl\_STOP\_fl}$ founders were first obtained through mixed crosses of mice that carried combinations of each transgene. *Rb1*$^{fl/fl}$;*Rosa26-tdTomato*$^{fl\_STOP\_fl}$ females were then crossed with *Blimp1-Cre*^{Tg};*Rb1*$^{fl/+}$ males to generate *Rb1* cKO males with fluorescence-labeled germ cells.

Histological analysis and immunofluorescence staining

Embryonic gonads and postnatal testes were fixed in 4% paraformaldehyde (PFA; Sigma-Aldrich, 158127) in PBS for 2 h at 4°C or Bouin's solution (Sigma-Aldrich, 15990-01) for 24 h at room temperature. Fixed samples were either stored in 70% ethanol at 4°C before paraffin embedding or dehydrated in 15% sucrose and frozen in optimal cutting temperature medium (Sakura, 4583). For all tissue blocks, 5 µm sections were cut using a Leica RM2255 automated microtome or Leica CM1950 cryostat.

For histomorphological analysis, paraffin sections from samples fixed in Bouin's solution were adhered to glass slides followed by incubation in xylene for dewaxing, rehydration by incubation in reducing concentrations of ethanol, and staining with Hematoxylin (Sigma-Aldrich, HHS16) and Eosin (Ricca, 2845-16). For immunofluorescence staining, antigen retrieval was achieved by incubation in an acidic (pH 6.0) solution of 10 mM sodium citrate (Amresco, 0101) and 0.05% Tween-20 (Sigma-Aldrich, P1379) for 20 min at 96°C. Non-specific antibody binding was blocked by incubating sections in a solution containing 2% bovine serum albumin (BSA; Thermo Fisher Scientific, BP1600) and 0.1% Triton X-100 (Sigma-Aldrich, T8787) in PBS at room temperature for 2 h. Sections were then incubated overnight at 4°C with primary antibody: rabbit anti-RB1 (1:150, Cell Signaling Technology, 9313), rabbit anti-phospho-RB1(Ser807/811) (1:100, Cell Signaling Technology, 9308), rat anti-TRA98 (1:500, Abcam, ab82527), rabbit anti-Ki67 (1:300, Abcam, ab15580), rabbit anti-cleaved caspase-3 (1:150, Cell Signaling Technology, 9661) or rabbit anti-STRA8 (1:4000, donated from Dr Mike Griswold, Washington State University, USA). Sections were washed in PBS and then incubated with a secondary antibody: TRITC-conjugated goat anti-rat IgG (1:500, Thermo Fisher Scientific, A11006) or FITC-conjugated goat anti rabbit IgG (1:500, Thermo Fisher Scientific, A11055, A11008) or Alexa Fluor 647-conjugated goat anti rabbit IgG (1:500, Thermo Fisher Scientific, A21245) at room temperature for 2 h. Sections were again washed in PBS and then coverslips mounted with medium containing DAPI (Vector Laboratories, H-1200). Images were captured using an Olympus IX51 or Leica DMi8 microscope.

Single-cell RNA sequencing

Single-cell suspensions were generated from E14.5 testes as described previously. Briefly, tissue was incubated in a solution of 5 ml 0.25% trypsin-EDTA (Thermo Fisher Scientific, 25200-056) and 2 ml deoxyribonuclease I solution (7 mg/ml; Sigma-Aldrich, DN25) with occasional pipetting at 37°C for a total of 10 min. Trypsin digestion was quenched by addition of fetal bovine serum (FBS; Thermo Fisher Scientific, 10438-034). The cell suspension was then passed through a 40 µm cell strainer and centrifuged at 600 ***g*** for 7 min at 4°C. Cells were then washed in DPBS-S [PBS with 1% FBS, 10 mM HEPES (Sigma-Aldrich, H0887), 1 mM sodium pyruvate (Thermo Fisher Scientific, 11360-070), 1 mg/ml glucose (Sigma-Aldrich, G7528), 1% penicillin/streptomycin (Thermo Fisher Scientific, 15140-122)]. tdTomato^{+} germ cells were isolated using an SH800 FACS machine (Sony Biotechnology). Germ cells were washed and resuspended in a solution of 0.04% non-acetylated BSA in PBS. The resulting cell suspension was loaded into a Chromium Controller (10x Genomics) and single-cell cDNA libraries were generated using v2 chemistry according to the manufacturer's protocol. A total of six libraries were pooled at proportions netting equal read depth and sequenced in the same lane on an Illumina HiSeq 4000 (Genomics & Cell Characterization Core Facility, University of Oregon, USA).

Raw base call files were demultiplexed using the 10x Genomics Cell Ranger pipeline and aligned to the mouse mm10 transcriptome. Six libraries totaling 7585 cells were imported into R (version 3.6.0) and analyzed with the Seurat 3.0 package. Using anchor integration, libraries were merged, normalized, scaled, and dimensionally reduced with default settings. For clustering, statistically significant principal components (PCs) were chosen based on a 'JackStraw' score ($P<0.05$). Determination of DEGs was performed with default settings. Single-cell trajectory analysis was constructed on integration of scRNA-seq data generated in the current study with GEO datasets GSE124904 and GSE119045 using the Monocle 2 package based on the top 1000 DEGs (Table S2, $P\leq0.05$) from the 11 clusters generated in Seurat 3.0. Gene Ontology assessment was conducted using the DAVID Bioinformatics Resource v6.8 (https://david.ncifcrf.gov/summary.jsp).

Apoptosis analysis

Assessment of apoptotic cells was achieved by scoring of cleaved CASPASE-3-positive germ cells in cross-sections of testes. Briefly, paraffin cross-sections mounted on glass slides were processed for

co-immunofluorescence staining of cleaved CASPASE-3 and TRA98 as described above and examined by fluorescent microscopy at 20× magnification. For each testis, three different cross-sections were examined, and digital images were captured. In each image, the number of germ cells and cleaved CASPASE-3-positive germ cells per seminiferous cord/tubule were counted to determine the percentage of the population that was apoptotic.

RNA isolation and quantitative real-time PCR

Total RNA was isolated using Trizol reagent (Thermo Fisher Scientific, 155996026) and reverse transcription was performed using a SuperScript III First-Strand kit (Thermo Fisher Scientific, 18080-051). Relative abundance of *Stra8* mRNA was measured using a 7500 Fast PCR System (Applied Biosystems) with Maxima SYBR Green/ROX qPCR Master Mix (Thermo Fisher Scientific, K0221) and normalization to mRNA levels of the housekeeping gene *Actb*. Primer sequences are listed in Table S4. Melt curve analysis was used to confirm the generation of a single amplicon and relative transcript levels were determined using the $2^{-\Delta\Delta ct}$ method.

Quantification and statistics

All quantitative data are presented as mean±s.e.m. and differences between experimental groups were determined statistically using the Student's *t*-test (independent-samples *t*-test) or nonparametric test (Mann–Whitney *U*-test) function of SPSS software (IBM Corporation, version 19.0) when the data were of normal distribution or non-normal distribution, respectively.

Competing interests

The authors declare no competing or financial interests.

Author contributions

Conceptualization: J.M.O., G.D., M.J.O., N.C.L., X.W.; Methodology: J.M.O., G.D., M.J.O., N.C.L., C.R.; Validation: G.D.; Formal analysis: J.M.O., G.D., M.J.O., N.C.L.; Investigation: J.M.O., G.D., M.J.O., N.C.L., C.R.; Resources: J.M.O.; Writing - original draft: J.M.O.; Writing - review & editing: J.M.O., G.D., M.J.O., N.C.L., C.R., X.W.; Supervision: J.M.O.; Project administration: J.M.O.; Funding acquisition: J.M.O.

Funding

This research was supported by grants from the Eunice Kennedy Shriver National Institute of Child Health and Human Development (HD061665 and HD094568 to J.M.O.), the National Key Basic Research Program (2018YFC1003302 to X.W.) and the National Natural Science Foundation of China (31872844 to X.W.). G.D. was supported by project C084 from the International Cooperation and Exchanges of Nanjing Medical University. Deposited in PMC for release after 12 months.

Data availability

Single-cell RNA-sequencing data are available in the NCBI Gene Expression Omnibus database under accession number GSE149223.

Peer review history

The peer review history is available online at
https://journals.biologists.com/dev/article-lookup/doi/10.1242/dev.194571

References

Aitken, R. J., Findlay, J. K., Hutt, K. J. and Kerr, J. B. (2011). Apoptosis in the germ line. *Reproduction* **141**, 139-150. doi:10.1530/REP-10-0232

Barton, L. J., LeBlanc, M. G. and Lehmann, R. (2016). Finding their way: themes in germ cell migration. *Curr. Opin. Cell Biol.* **42**, 128-137. doi:10.1016/j.ceb.2016.07.007

Bejarano, I., Rodriguez, A. B. and Pariente, J. A. (2018). Apoptosis is a demanding selective tool during the development of fetal male germ cells. *Front. Cell Dev. Biol.* **6**, 65. doi:10.3389/fcell.2018.00065

Bellve, A. R., Cavicchia, J. C., Millette, C. F., O'Brien, D. A., Bhatnagar, Y. M. and Dym, M. (1977). Spermatogenic cells of the prepuberal mouse. Isolation and morphological characterization. *J. Cell Biol.* **74**, 68-85.

Borgel, J., Guibert, S., Li, Y., Chiba, H., Schubeler, D., Sasaki, H., Forne, T. and Weber, M. (2010). Targets and dynamics of promoter DNA methylation during early mouse development. *Nat. Genet.* **42**, 1093-1100. doi:10.1038/ng.708

Burke, J. R., Hura, G. L. and Rubin, S. M. (2012). Structures of inactive retinoblastoma protein reveal multiple mechanisms for cell cycle control. *Genes Dev.* **26**, 1156-1166. doi:10.1101/gad.189837.112

Chan, F., Oatley, M. J., Kaucher, A. V., Yang, Q. E., Bieberich, C. J., Shashikant, C. S. and Oatley, J. M. (2014). Functional and molecular features of the Id4+ germline stem cell population in mouse testes. *Genes Dev.* **28**, 1351-1362. doi:10.1101/gad.240465.114

DeGregori, J., Kowalik, T. and Nevins, J. R. (1995). Cellular targets for activation by the E2F1 transcription factor include DNA synthesis- and G1/S-regulatory genes. *Mol. Cell. Biol.* **15**, 4215-4224. doi:10.1128/MCB.15.8.4215

de Rooij, D. G. and Russell, L. D. (2000). All you wanted to know about spermatogonia but were afraid to ask. *J. Androl.* **21**, 776-798.

Dick, F. A. and Rubin, S. M. (2013). Molecular mechanisms underlying RB protein function. *Nat. Rev. Mol. Cell Biol.* **14**, 297-306. doi:10.1038/nrm3567

Folmes, C. D., Dzeja, P. P., Nelson, T. J. and Terzic, A. (2012). Metabolic plasticity in stem cell homeostasis and differentiation. *Cell Stem Cell* **11**, 596-606. doi:10.1016/j.stem.2012.10.002

Gallardo, T., Shirley, L., John, G. B. and Castrillon, D. H. (2007). Generation of a germ cell-specific mouse transgenic Cre line, Vasa-Cre. *Genesis* **45**, 413-417. doi:10.1002/dvg.20310

Goolam, M., Xypolita, M. E., Costello, I., Lydon, J. P., DeMayo, F. J., Bikoff, E. K., Robertson, E. J. and Mould, A. W. (2020). The transcriptional repressor Blimp1/PRDM1 regulates the maternal decidual response in mice. *Nat. Commun.* **11**, 2782. doi:10.1038/s41467-020-16603-z

Guo, J., Grow, E. J., Yi, C., Mlcochova, H., Maher, G. J., Lindskog, C., Murphy, P. J., Wike, C. L., Carrell, D. T., Goriely, A. et al. (2017). Chromatin and Single-Cell RNA-Seq Profiling Reveal Dynamic Signaling and Metabolic Transitions during Human Spermatogonial Stem Cell Development. *Cell Stem Cell* **21**, 533-546.e536. doi:10.1016/j.stem.2017.09.003

Hamer, G. and de Rooij, D. G. (2018). Mutations causing specific arrests in the development of mouse primordial germ cells and gonocytes. *Biol. Reprod.* **99**, 75-86. doi:10.1093/biolre/ioy075

Hayashi, Y., Otsuka, K., Ebina, M., Igarashi, K., Takehara, A., Matsumoto, M., Kanai, A., Igarashi, K., Soga, T. and Matsui, Y. (2017). Distinct requirements for energy metabolism in mouse primordial germ cells and their reprogramming to embryonic germ cells. *Proc. Natl. Acad. Sci. USA* **114**, 8289-8294. doi:10.1073/pnas.1620915114

Helsel, A. R., Oatley, M. J. and Oatley, J. M. (2017). Glycolysis-optimized conditions enhance maintenance of regenerative integrity in mouse spermatogonial stem cells during long-term culture. *Stem Cell Reports* **8**, 1430-1441. doi:10.1016/j.stemcr.2017.03.004

Hu, Y. C., de Rooij, D. G. and Page, D. C. (2013). Tumor suppressor gene Rb is required for self-renewal of spermatogonial stem cells in mice. *Proc. Natl. Acad. Sci. USA* **110**, 12685-12690. doi:10.1073/pnas.1311548110

Kluin, P. M. and de Rooij, D. G. (1981). A comparison between the morphology and cell kinetics of gonocytes and adult type undifferentiated spermatogonia in the mouse. *Int. J. Androl.* **4**, 475-493. doi:10.1111/j.1365-2605.1981.tb00732.x

Kurimoto, K., Yabuta, Y., Ohinata, Y., Shigeta, M., Yamanaka, K. and Saitou, M. (2008). Complex genome-wide transcription dynamics orchestrated by Blimp1 for the specification of the germ cell lineage in mice. *Genes Dev.* **22**, 1617-1635. doi:10.1101/gad.1649908

Law, N. C., Oatley, M. J. and Oatley, J. M. (2019). Developmental kinetics and transcriptome dynamics of stem cell specification in the spermatogenic lineage. *Nat. Commun.* **10**, 2787. doi:10.1038/s41467-019-10596-0

Lawson, K. A., Dunn, N. R., Roelen, B. A., Zeinstra, L. M., Davis, A. M., Wright, C. V., Korving, J. P. and Hogan, B. L. (1999). Bmp4 is required for the generation of primordial germ cells in the mouse embryo. *Genes Dev.* **13**, 424-436. doi:10.1101/gad.13.4.424

LeCouter, J. E., Whyte, P. F. and Rudnicki, M. A. (1996). Cloning and expression of the Rb-related mouse p130 mRNA. *Oncogene* **12**, 1433-1440.

Li, Y. and Sasaki, H. (2011). Genomic imprinting in mammals: its life cycle, molecular mechanisms and reprogramming. *Cell Res.* **21**, 466-473. doi:10.1038/cr.2011.15

Li, Z., Yu, J., Hosohama, L., Nee, K., Gkountela, S., Chaudhari, S., Cass, A. A., Xiao, X. and Clark, A. T. (2015). The Sm protein methyltransferase PRMT5 is not required for primordial germ cell specification in mice. *EMBO J.* **34**, 748-758. doi:10.15252/embj.201489319

Lin, Y. T. and Capel, B. (2015). Cell fate commitment during mammalian sex determination. *Curr. Opin. Genet. Dev.* **32**, 144-152. doi:10.1016/j.gde.2015.03.003

Lord, T. and Nixon, B. (2020). Metabolic Changes Accompanying Spermatogonial Stem Cell Differentiation. *Dev. Cell* **52**, 399-411. doi:10.1016/j.devcel.2020.01.014

Ly, L., Chan, D. and Trasler, J. M. (2015). Developmental windows of susceptibility for epigenetic inheritance through the male germline. *Semin. Cell Dev. Biol.* **43**, 96-105. doi:10.1016/j.semcdb.2015.07.006

Magnusdottir, E., Dietmann, S., Murakami, K., Gunesdogan, U., Tang, F., Bao, S., Diamanti, E., Lao, K., Gottgens, B. and Azim Surani, M. (2013). A tripartite transcription factor network regulates primordial germ cell specification in mice. *Nat. Cell Biol.* **15**, 905-915. doi:10.1038/ncb2798

Miller, I., Min, M., Yang, C., Tian, C., Gookin, S., Carter, D. and Spencer, S. L. (2018). Ki67 is a Graded rather than a binary marker of proliferation versus quiescence. *Cell Rep* **24**, 1105-1112.e1105. doi:10.1016/j.celrep.2018.06.110

Murphey, P., McLean, D. J., McMahan, C. A., Walter, C. A. and McCarrey, J. R. (2013). Enhanced genetic integrity in mouse germ cells. *Biol. Reprod.* **88**, 6. doi:10.1095/biolreprod.112.103481

Nagano, R., Tabata, S., Nakanishi, Y., Ohsako, S., Kurohmaru, M. and Hayashi, Y. (2000). Reproliferation and relocation of mouse male germ cells (gonocytes) during prespermatogenesis. *Anat. Rec.* **258**, 210-220. doi:10.1002/(SICI)1097-0185(20000201)258:2<210::AID-AR10>3.0.CO;2-X

Nguyen, D. H., Jaszczak, R. G. and Laird, D. J. (2019). Heterogeneity of primordial germ cells. *Curr. Top. Dev. Biol.* **135**, 155-201. doi:10.1016/bs.ctdb.2019.04.009

Nguyen, D. H., Soygur, B., Peng, S. P., Malki, S., Hu, G. and Laird, D. J. (2020). Apoptosis in the fetal testis eliminates developmentally defective germ cell clones. *Nat. Cell Biol.* **22**, 1423-1435. doi:10.1038/s41556-020-00603-8

Nicholas, C. R., Xu, E. Y., Banani, S. F., Hammer, R. E., Hamra, F. K. and Reijo Pera, R. A. (2009). Characterization of a Dazl-GFP germ cell-specific reporter. *Genesis* **47**, 74-84. doi:10.1002/dvg.20460

Nicholls, P. K., Schorle, H., Naqvi, S., Hu, Y. C., Fan, Y., Carmell, M. A., Dobrinski, I., Watson, A. L., Carlson, D. F., Fahrenkrug, S. C. et al. (2019). Mammalian germ cells are determined after PGC colonization of the nascent gonad. *Proc. Natl. Acad. Sci. USA* **116**, 25677-25687. doi:10.1073/pnas.1910733116

Oatley, J. M. and Brinster, R. L. (2008). Regulation of spermatogonial stem cell self-renewal in mammals. *Annu. Rev. Cell Dev. Biol.* **24**, 263-286. doi:10.1146/annurev.cellbio.24.110707.175355

Ohinata, Y., Payer, B., O'Carroll, D., Ancelin, K., Ono, Y., Sano, M., Barton, S. C., Obukhanych, T., Nussenzweig, M., Tarakhovsky, A. et al. (2005). Blimp1 is a critical determinant of the germ cell lineage in mice. *Nature* **436**, 207-213. doi:10.1038/nature03813

Richardson, B. E. and Lehmann, R. (2010). Mechanisms guiding primordial germ cell migration: strategies from different organisms. *Nat. Rev. Mol. Cell Biol.* **11**, 37-49. doi:10.1038/nrm2815

Rivera-Perez, J. A. and Magnuson, T. (2005). Primitive streak formation in mice is preceded by localized activation of Brachyury and Wnt3. *Dev. Biol.* **288**, 363-371. doi:10.1016/j.ydbio.2005.09.012

Rohwedel, J., Sehlmeyer, U., Shan, J., Meister, A. and Wobus, A. M. (1996). Primordial germ cell-derived mouse embryonic germ (EG) cells in vitro resemble undifferentiated stem cells with respect to differentiation capacity and cell cycle distribution. *Cell Biol. Int.* **20**, 579-587. doi:10.1006/cbir.1996.0076

Runyan, C., Schaible, K., Molyneaux, K., Wang, Z., Levin, L. and Wylie, C. (2006). Steel factor controls midline cell death of primordial germ cells and is essential for their normal proliferation and migration. *Development* **133**, 4861-4869. doi:10.1242/dev.02688

Saitou, M. and Yamaji, M. (2012). Primordial germ cells in mice. *Cold Spring Harb. Perspect Biol.* **4**, a008375. doi:10.1101/cshperspect.a008375

Seki, Y., Yamaji, M., Yabuta, Y., Sano, M., Shigeta, M., Matsui, Y., Saga, Y., Tachibana, M., Shinkai, Y. and Saitou, M. (2007). Cellular dynamics associated with the genome-wide epigenetic reprogramming in migrating primordial germ cells in mice. *Development* **134**, 2627-2638. doi:10.1242/dev.005611

Sivakumar, S. and Gorbsky, G. J. (2015). Spatiotemporal regulation of the anaphase-promoting complex in mitosis. *Nat. Rev. Mol. Cell Biol.* **16**, 82-94. doi:10.1038/nrm3934

Sorrentino, E., Nazzicone, V., Farini, D., Campagnolo, L. and De Felici, M. (2007). Comparative transcript profiles of cell cycle-related genes in mouse primordial germ cells, embryonic stem cells and embryonic germ cells. *Gene Expr. Patterns* **7**, 714-721. doi:10.1016/j.modgep.2007.02.002

Spiller, C. M., Wilhelm, D. and Koopman, P. (2010). Retinoblastoma 1 protein modulates XY germ cell entry into G1/G0 arrest during fetal development in mice. *Biol. Reprod.* **82**, 433-443. doi:10.1095/biolreprod.109.078691

Tam, P. P. and Snow, M. H. (1981). Proliferation and migration of primordial germ cells during compensatory growth in mouse embryos. *J. Embryol. Exp. Morphol.* **64**, 133-147.

Vanhoutteghem, A., Messiaen, S., Herve, F., Delhomme, B., Moison, D., Petit, J. M., Rouiller-Fabre, V., Livera, G. and Djian, P. (2014). The zinc-finger protein basonuclin 2 is required for proper mitotic arrest, prevention of premature meiotic initiation and meiotic progression in mouse male germ cells. *Development* **141**, 4298-4310. doi:10.1242/dev.112888

Varuzhanyan, G., Rojansky, R., Sweredoski, M. J., Graham, R. L., Hess, S., Ladinsky, M. S. and Chan, D. C. (2019). Mitochondrial fusion is required for spermatogonial differentiation and meiosis. *Elife* **8**, e51601. doi:10.7554/eLife.51601

Vega-Naredo, I., Loureiro, R., Mesquita, K. A., Barbosa, I. A., Tavares, L. C., Branco, A. F., Erickson, J. R., Holy, J., Perkins, E. L., Carvalho, R. A. et al. (2014). Mitochondrial metabolism directs stemness and differentiation in P19 embryonal carcinoma stem cells. *Cell Death Differ.* **21**, 1560-1574. doi:10.1038/cdd.2014.66

Vergouwen, R. P., Jacobs, S. G., Huiskamp, R., Davids, J. A. and de Rooij, D. G. (1991). Proliferative activity of gonocytes, Sertoli cells and interstitial cells during testicular development in mice. *J. Reprod Fertil.* **93**, 233-243. doi:10.1530/jrf.0.0930233

Wang, R. A., Nakane, P. K. and Koji, T. (1998). Autonomous cell death of mouse male germ cells during fetal and postnatal period. *Biol. Reprod.* **58**, 1250-1256. doi:10.1095/biolreprod58.5.1250

Western, P. S., Miles, D. C., van den Bergen, J. A., Burton, M. and Sinclair, A. H. (2008). Dynamic regulation of mitotic arrest in fetal male germ cells. *Stem Cells* **26**, 339-347. doi:10.1634/stemcells.2007-0622

Yamaji, M., Seki, Y., Kurimoto, K., Yabuta, Y., Yuasa, M., Shigeta, M., Yamanaka, K., Ohinata, Y. and Saitou, M. (2008). Critical function of Prdm14 for the establishment of the germ cell lineage in mice. *Nat. Genet.* **40**, 1016-1022. doi:10.1038/ng.186

Yang, Q. E., Gwost, I., Oatley, M. J. and Oatley, J. M. (2013). Retinoblastoma protein (RB1) controls fate determination in stem cells and progenitors of the mouse male germline. *Biol. Reprod.* **89**, 113. doi:10.1095/biolreprod.113.113159

Yang, Q. E., Nagaoka, S. I., Gwost, I., Hunt, P. A. and Oatley, J. M. (2015). Inactivation of retinoblastoma protein (Rb1) in the oocyte: evidence that dysregulated follicle growth drives ovarian teratoma formation in mice. *PLoS Genet.* **11**, e1005355. doi:10.1371/journal.pgen.1005355

Yoshimizu, T., Sugiyama, N., De Felice, M., Yeom, Y. I., Ohbo, K., Masuko, K., Obinata, M., Abe, K., Scholer, H. R. and Matsui, Y. (1999). Germline-specific expression of the Oct-4/green fluorescent protein (GFP) transgene in mice. *Dev. Growth Differ.* **41**, 675-684. doi:10.1046/j.1440-169x.1999.00474.x

Zamboni, L. and Merchant, H. (1973). The fine morphology of mouse primordial germ cells in extragonadal locations. *Am. J. Anat.* **137**, 299-335. doi:10.1002/aja.1001370305

Zhou, Q., Nie, R., Li, Y., Friel, P., Mitchell, D., Hess, R. A., Small, C. and Griswold, M. D. (2008). Expression of stimulated by retinoic acid gene 8 (Stra8) in spermatogenic cells induced by retinoic acid: an in vivo study in vitamin A-sufficient postnatal murine testes. *Biol. Reprod.* **79**, 35-42. doi:10.1095/biolreprod.107.066795